Multiple Mean Models of Statistical Shape and Probability Priors for Automatic Prostate Segmentation.

Soumya Ghose, Arnau Oliver, Robert Marti, Xavier Llado, Jordi Freixenet, Jhimli Mitra, Joan C. Vilanova, Josep Comet, Fabrice Mériaudeau

Multiple Mean Models of Statistical Shape and Probability Priors for Automatic Prostate Segmentation

Soumya Ghose[1,2], Arnau Oliver[1], Robert Martí[1], Xavier Lladó[1], Jordi Freixenet[1], Jhimli Mitra[1,2], Joan C. Vilanova[3], Josep Comet[4] and Fabrice Meriaudeau[2]

[1] Computer Vision and Robotics Group, University of Girona, Campus Montilivi, Edifici P-IV, Av. Lluís Santaló , s/n, 17071 Girona, Spain
[2] Laboratoire Le2I - UMR CNRS 5158, Université de Bourgogne, 12 Rue de la Fonderie, 71200 Le Creusot, France
[3] Girona Magnetic Resonance Imaging Center, Girona, Spain
[4] University Hospital Dr. Josep Trueta, Girona, Spain.

Abstract. Low contrast of the prostate gland, heterogeneous intensity distribution inside the prostate region, imaging artifacts like shadow regions, speckle and significant variations in prostate shape, size and inter dataset contrast in Trans Rectal Ultrasound (TRUS) images challenge computer aided automatic or semi-automatic segmentation of the prostate. In this paper, we propose a probabilistic framework for automatic initialization and propagation of multiple mean parametric models derived from principal component analysis of shape and posterior probability information of the prostate region to segment the prostate. Unlike traditional statistical models of shape and intensity priors we use posterior probability of the prostate region to build our texture model of the prostate and use the information in initialization and propagation of the mean model. Furthermore, multiple mean models are used compared to a single mean model to improve segmentation accuracies. The proposed method achieves mean Dice Similarity Coefficient (DSC) value of 0.97±0.01, and mean Mean Absolute Distance (MAD) value of 0.49±0.20 mm when validated with 23 datasets with considerable shape, size, and intensity variations, in a leave-one-patient-out validation framework. The model achieves statistically significant t-test p-value$<$0.0001 in mean DSC and mean MAD values compared to traditional statistical models of shape and texture. Introduction of the probabilistic information of the prostate region and multiple mean models into the traditional statistical shape and texture model framework, significantly improve the segmentation accuracies.

Keywords: Prostate Segmentation, Bayesian Framework, Multiple Statistical Shape and Posterior Probability Models.

1 Introduction

An estimated 913,000 people worldwide were diagnosed with prostate cancer [1] in 2008. TRUS guided biopsy is commonly used to diagnose prostate cancer due to inexpensive real-time nature of the system and simplicity [15]. Accurate prostate segmentation in TRUS may aid in radiation therapy planning, motion monitoring, biopsy needle placement and multimodal image fusion between TRUS and magnetic resonance imaging (MRI) to improve malignant tissue extraction during biopsy [15]. However, accurate computer aided prostate segmentation from TRUS images encounters considerable challenges due to low contrast of TRUS images, heterogeneous intensity distribution inside the prostate gland, speckle, shadow artifacts, and presence of micro-calcifications inside the prostate. There is no global characterization for the prostate and the non-prostate regions in terms of pixel intensities and region appearance [15]. Moreover, inter patient prostate shape, size and deformation may vary significantly.

Often deformable models and statistical shape models are used in prostate segmentation. For example Badiel et al. [2] used a deformable model of warping ellipse and Ladak et al. [11] used discrete dynamic contour to achieve semi-automatic prostate segmentation. However, TRUS guided procedures should necessarily be automatic. Shen et al. [14] and Zhan et al. [16] presented an automatic method that incorporated a priori shape and texture information from Gabor filters to produce accurate prostate segmentation. However, the method is computationally expensive and probably unsuitable for TRUS guided prostate intervention [15]. In recent years Cosio et al. [6] reported an automatic method for prostate segmentation with active shape models [4]. However, the optimization framework of genetic algorithm used is computationally intensive and unsuitable for TRUS guided intervention.

To address the challenges involved with prostate segmentation in TRUS images we propose a multi-resolution framework using multiple mean parametric models derived from Principal Component Analysis (PCA) of prostate shape and posterior probabilistic values of the prostate region in TRUS images. The performance of our method is compared with the traditional AAM [5] and also with our previous work [9]. Compared to the use of intensity and one mean model as in [5] and to the use of texture from Haar wavelet features in [9], posterior probabilistic information of the prostate region obtained in a Bayesian framework is used to train, initialize and propagate our multiple statistical models of shape and texture. Statistically significant improvement is achieved with the use of multiple mean models in the Bayesian framework when validated with 23 datasets, that have significant shape, size, and contrast variations of the prostate, in leave-one-patient-out validation framework. Experimental results show that our method is unaffected by low contrast, heterogeneity of intensity distribution inside the prostate, speckle, shadow artifacts, micro-calcifications, and significant shape, size and intensity variations of the prostate gland between the datasets. Shen et al. [14] and Zhan et al. [16] proposed to use Gabor filters to model prostate texture and reduce heterogeneity of the prostate region in TRUS images. However, they often concluded that texture information inside the prostate region is

unreliable. Hence, we adopt a probabilistic modeling of the prostate region based on both positional information and intensity distribution inside the prostate to reduce heterogeneity. The key contributions of this work are:

- The use of posterior probability information of the prostate region to build the statistical model of texture.
- Using such information in training, automatic initialization and propagation of the mean models.
- The selection of a mean model depending on the error of fitting of the posterior probability information of the prostate region for accurate segmentation.

2 Proposed Segmentation Framework

The proposed method is developed on three major components: 1) Bayesian framework to determine posterior probability of a pixel being prostate, 2) adapting multiple statistical models of shape and texture priors to incorporate the posterior probabilities of the prostate region for training, initialization and propagation of the parametric model and 3) selection of one of the mean models depending on the error of fitting of the posterior probabilities to segment the prostate. We present the Bayesian framework for determining posterior probability of the prostate region first followed by our statistical shape and probability model of the prostate region. The optimization framework is addressed thereafter, and finally the grouping of the datasets for building multiple mean models and selection of one among the mean models for segmentation is discussed.

2.1 Bayesian Formulation

In traditional AAM [5], the point distribution model (PDM) [4] of the contour is aligned to a common reference frame by generalized Procrustes analysis [10]. Intensities are warped into correspondence using a piece wise affine warp and sampled from a shape-free reference. Intensity distribution inside the prostate region may vary significantly from one dataset to another depending on the parameters of acquisition and nature of the prostate tissue of a patient. Hence, the use of intensity distribution of the prostate region to build the texture model, as in traditional AAM introduces larger variabilities producing an inaccurate texture model which adversely affects segmentation results. To reduce inter dataset intensity variabilities and intensity variabilities inside the prostate region, we propose to determine the posterior probability of the image pixels being prostate in a Bayesian framework and use PCA of the posterior probabilities of the prostate region to build our texture model. We use K-means clustering to roughly cluster the pixels into two classes (prostate and non-prostate) from the intensities. The class means and standard deviations obtained from this rough clustering are then used as the initial estimates in an expectation maximization (EM) [8] framework to determine the probability of a pixel being prostate from intensities. The E-step assigns the probabilities to the pixels depending on the

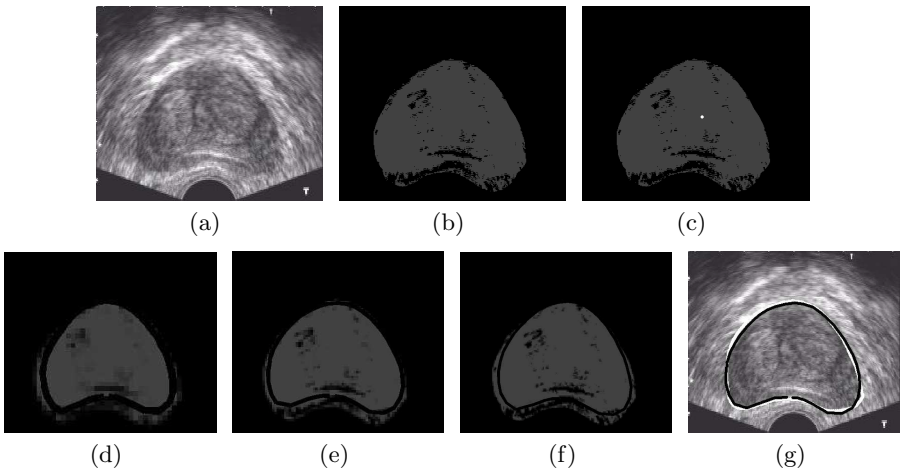

Fig. 1. Bayesian framework (a) TRUS image of a prostate (b) a posteriori of a pixel being prostate, (c) centroid (white dot) computed from posterior probability values for AAM initialization. On initialization, the AAM segments prostate in a multi-resolution framework 1(d), 1(e) and 1(f) to give final segmentation 1(g).

current mean and standard deviation values of the classes, while in M-step the means and standard deviation values are re-estimated. Maximum a posteriori estimates of the class means and standard deviations are used to soft cluster the pixels.

The likelihood of a pixel location in an image being prostate is obtained by normalizing the ground truth values of all the pixels for all the training images as

$$P\left(x_{ps}|C_{prs}\right) = \frac{1}{N}\sum_{i=1}^{N} GT_i \tag{1}$$

where $P\left(x_{ps}|C_{prs}\right)$ gives the probability of a pixel position being prostate with x_{ps} being the pixel location and C_{prs} denoting prostate. GT_i represents ground truth of the training images with N the total number of ground truth images. In our model the class prior probability is estimated from the frequency of the pixels (x) belonging to a class as

$$P\left(C_{Prostate}\right) = \frac{\sum_{i=1}^{pnm} x_i}{\sum_{j=1}^{m} x_j} \tag{2}$$

where $P\left(C_{Prostate}\right)$ gives the class prior probability of being prostate, x_i represents the pixels belonging to prostate region (total given by pnm) and x_j represents the pixels in all training images (given by m). The probabilities of intensity (being prostate) obtained in EM framework, location (being prostate) and class prior probability (prostate class) are used in a Bayesian framework to determine posterior probability of a pixel being prostate (Fig. 1(b)). According

to Bayes rule,

$$P\left(C_i|X\right) = \frac{P\left(X|C_i\right)P\left(C_i\right)}{P\left(X\right)} \tag{3}$$

the posterior probability distribution $P\left(C_i|\,X\right)$ of a class is given by the prior $P\left(C_i\right)$ (i.e. $P\left(C_{Prostate}\right)$) and the likelihood $P\left(X|C_i\right)$. $P\left(X\right)$ being equal for all classes can be removed from the formulation. Considering class conditional independence (as the probability of a pixel intensity being prostate is independent of the pixel location in the image and vice versa), the likelihood could be formalized as,

$$P\left(X|C_i\right) = P\left(x_{ps}|C_{prs}\right).P\left(x_{in}|C_{prs}\right) \tag{4}$$

In equation (4) the likelihood $P\left(X|C_i\right)$ is obtained from the product of the probability of a pixel intensity being prostate ($P\left(x_{in}|C_{prs}\right)$) obtained from EM framework (x_{in} being pixel intensity) and the probability of a pixel location being prostate ($P\left(x_{ps}|C_{prs}\right)$) obtained from (1). Our approach of using pixel location for determining prior position information of the prostate is based on the works of Cosio et al. [6] and Shen et al. [14]. Both used prior prostate location information in TRUS images for automatic initialization of their model. Cosio et al. [6] used a 3D feature vector of pixel location and intensity value to classify and localize prostate in TRUS images for initialization of their model. Similarly, Shen et al. [14] proposed to use the relative position of the prostate with respect to the TRUS probe (located at the center of the base line of the TRUS image) for initialization. These methods prove that prostate location in TRUS images is not random and provides meaningful information. Hence, we exploit the location information of the prostate in TRUS images in our Bayesian framework to determine the posterior probability of the prostate region.

2.2 Statistical Shape and Texture Model

The process of building the parametric statistical model of shape and texture variations involves the task of building a shape model, a texture model, and consecutively a combined model of texture and shape and prior learning of the optimization space from the combined model perturbation. To build the shape model, a PDM [5] is built by equal angle sampling of the prostate contours to determine the landmarks automatically. The PDM of the contours are aligned to a common reference frame by generalized Procrustes analysis [10]. PCA of the aligned PDMs identifies the principal modes of shape variations. Posteriori probabilistic information (of pixels being prostate) of the segmented region are warped into correspondence using a piece wise affine warp and sampled from shape free reference similar to the AAM [5]. PCA of the posterior probabilities from (4) is used to identify their principal modes of variation. The model may be formalized in the following manner. Let s and t represent the shape and posterior probability models, then

$$s = \overline{s} + \Phi_s\theta_s, \quad t = \overline{t} + \Phi_t\theta_t \tag{5}$$

where $\overline{s}$ and $\overline{t}$ denote the mean shape and posterior probability information respectively, then Φ_s and Φ_t contain the first p eigenvectors (obtained from 98% of total variations) of the estimated joint dispersion matrix of shape and posterior probability information and θ represent the corresponding eigenvalues. The model of shape and posterior probability variations are combined in a linear framework as,

$$b = \begin{bmatrix} W\theta_s \\ \theta_t \end{bmatrix} = \begin{bmatrix} W\Phi_s^T(s - \overline{s}) \\ \Phi_t^T(t - \overline{t}) \end{bmatrix} \tag{6}$$

where W denotes a weight factor (determined as in AAM [5]) coupling the shape and the probability space. A third PCA of the combined model ensures the reduction in redundancy of the combined model, and is given as,

$$b = Vc \tag{7}$$

where V is the matrix of eigenvectors and c the appearance parameters.

2.3 Optimization and Segmentation of a New Instance

In our model, we incorporate AAM optimization proposed by Cootes et al. [5]. The objective function of our model is similar to AAM. However, instead of minimizing the sum of squared difference of intensity between the mean model and target image, we minimize the sum of squared difference of the posterior probability of the mean model and the target image. The prior knowledge of the optimization space is acquired by perturbing the combined model with known model parameters and perturbing the pose (translation, scale and rotation) parameters. A linear relationship between the perturbation of the combined model (δc) and the residual posterior probability values (δt) (obtained from the sum of squared difference between the posterior probability of the mean model and the target image), and between the perturbation of the pose parameters (δp) and the residual posterior probability values are acquired in a multivariate regression framework as,

$$\delta c = R_c \delta t, \quad \delta p = R_p \delta t \tag{8}$$

R_c and R_p refer to the correlation coefficients. Given a test image, posterior probability values of the pixels being prostate is determined in the Bayesian framework 2.1. The sum of squared difference of the posterior probability values with the mean model is used to determine the residual value δt. The combined model (δc) and the pose parameters (δp) are then updated using (8) to generate a new shape, and combined model and hence, new posterior probabilities. The process continues in an iterative manner until the difference with the target image remains unchanged.

2.4 Multiple Mean Models

Statistical shape and texture model assumes the shape and the texture spaces to be Gaussian. However, inter patient prostate shape and their intensities may vary significantly. In such circumstances, a single Gaussian mean model is inefficient to

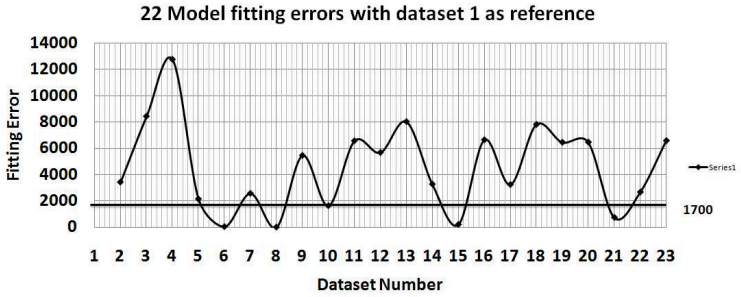

Fig. 2. Mean models fitting errors for with dataset 1 as reference.

capture the variations of shape and texture spaces. To address this problem, we propose to use multiple Gaussian mean models. The sum of squared differences of the posterior probabilities between the mean models and a given test image is recorded as the fitting error after the final segmentation with each of the mean model. The segmentation results of the mean model with the least fitting error is considered as the optimized segmentation.

The scheme of building the mean models is as follows; initially the 1st dataset is chosen as the reference to register datasets 3 to 23 to produce a mean model of shape and texture. This mean model is used to test dataset 2. The sum of squared difference of the posterior probabilities between the mean model and dataset 2 is recorded as fitting error after the final segmentation. Likewise, with the fixed reference (dataset 1), we build the second mean model registering datasets 2 and 4-23 to test on dataset 3 and record the fitting error. The process is repeated for all datasets from 4-23. This provides 22 model fitting errors for the test datasets with dataset 1 as reference (Fig. 2). Consequently, the reference dataset is changed from 2 through 23 and the entire process is repeated for all the datasets (23 in total). The entire procedure yields 23 graphs of model fitting errors (one for each dataset).

We have analyzed these 23 model fitting error graphs and have observed that with less fitting error (< 2000 units, where units signifies the sum of squared differences of the probability values of the prostate region between the mean model and the target image) we have higher accuracy in segmentation (in terms of Dice similarity coefficient, mean absolute distance etc.). This is not surprising considering the fact that the objective function of our optimization framework tries to minimize the fitting error between the mean model and target image with respect to the pose parameters. Hence, an increase in fitting error indicates a reduction in segmentation accuracies. An empirical error value is determined from these graphs, above which, the segmentation accuracy is reduced (in our case the threshold value is 1700 units). The reference dataset that has a fitting error less than the empirical value for maximum number of test datasets is identified (dataset 1 in our case). The datasets below this fitting error are grouped together (datasets 1, 6, 8, 10, 15 and 21(Fig. 2)) and are removed from

Table 1. Prostate segmentation quantitative comparison (HD, MAD and MaxD in mm, Spec., Sens., and Acc., are for Specificity, Sensitivity and Accuracy respectively.) Statistically significant values are italicized

Method	DSC	HD	MAD	MaxD	Spec.	Sens.	Acc.
AAM [5]	0.92±0.04	3.80±1.98	1.26±0.76	3.81±2.00	0.91±0.04	0.98±0.01	0.97±0.05
Ghose et al. [9]	0.94±0.03	2.59±1.21	0.91±0.44	2.64±1.19	0.91±0.04	0.98±0.01	0.97±0.05
B-AAM	0.95±0.06	2.53±1.94	0.87±1.23	2.35±2.10	0.92±0.04	0.97±0.04	0.97±0.03
Our Method	*0.97±0.01*	*1.78±0.73*	*0.49±0.20*	1.72±0.74	0.95±0.01	0.99±0.00	0.98±0.00

further grouping. The process is repeated until all the datasets are grouped. These groups of datasets provide individual mean models (5 mean models in our case). However, increasing the number of mean models (decreasing the fitting error threshold) improves segmentation accuracy with additional computational time. Hence, the choice of optimum number of mean models depends on the segmentation accuracy and computational time requirement of the process.

3 Experimental Results

We have validated the accuracy and robustness of our method with 46 axial mid gland TRUS images of the prostate with a resolution of 348×237 pixels from 23 prostate datasets in a leave-one-patient-out evaluation strategy. During validation, a test dataset is removed and 5 mean model are built with remaining 22 datasets. All the 5 mean models are applied to segment the test dataset. The mean model with the least fitting error is selected for accurate segmentation. The ground truth for the experiments are prepared in a schema similar to MICCAI prostate challenge 2009 [13], where manual segmentations performed by an expert radiologist are validated by an experienced urologist. Both doctors have over 15 years of experience in dealing with prostate anatomy, prostate segmentation, and ultrasound guided biopsies. We have used most of the popular prostate segmentation evaluation metrics like DSC, 95% Hausdorff Distance (HD) [13], MAD [15], Maximum Distance (MaxD) [12], specificity [7], sensitivity, and accuracy [2] to evaluate our method. Furthermore, the results are compared with the traditional AAM proposed by Cootes et al. [5], to our previous work [9] and to B-AAM (that uses posterior probability of the prostate region and a single mean model for segmentation). It is observed from Table 1 that, a probabilistic representation of the prostate texture in TRUS images and using multiple mean models significantly improves segmentation accuracy when compared to traditional AAM and to [9]. We used posterior probability information for automatic initialization and training of our statistical shape and texture model. As opposed to manual initialization of traditional AAM and in [9], our model is

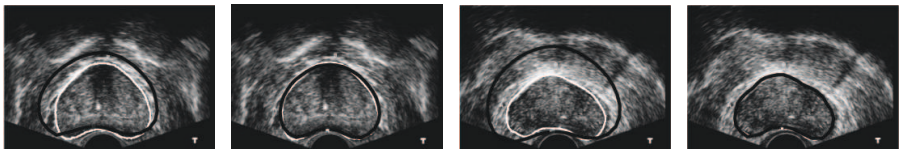

(a) (b) (c) (d)

Fig. 3. (a), (c) Segmentation without multiple mean model (B-AAM), (b), (d) Segmentation with multiple mean model.

initialized automatically. We achieved a statistically significant improvement in t-test p-value$<$0.0001 for DSC, HD and MAD compared to traditional AAM [5] and to [9]. A high DSC value and low values of contour error metrics of HD and MAD are all equally important in determining the segmentation accuracy of an algorithm. In this context, we obtained better segmentation accuracies compared to [5] and [9]. As observed in Table 1 B-AAM produces better result compared to AAM justifying the use of posterior probability of the prostate region instead of intensity. However, our model which uses both posterior probability and multiple mean models produces superior results compared to B-AAM, suggesting that use of both posterior probability and multiple mean models are essential to improve segmentation accuracies. Quantitative improvement in segmentation accuracy with multiple mean model is evident from the last two rows in Table 1. Qualitative improvement in segmentation accuracy compared to B-AAM is illustrated in Fig. 3 for two datasets. In Fig. 3, we observe that segmentation accuracy of our model (in Fig. 3(b) and Fig. 3(d)) is better compared to B-AAM (in Fig. 3(a) and Fig. 3(c)). Improved qualitative results with our method compared to traditional AAM [5] are illustrated in Fig. 4. Our method is implemented in Matlab 7 on an Intel Core 2 Duo T5250, 1.5 GHz processor and 2 GB RAM. The mean segmentation time of the method is 5.97$\pm$0.55 seconds with an unoptimized Matlab code. Even with an unoptimized Matlab code in Table 2 we observe that our mean segmentation time is comparable to [3], better than [14] and [6] and inferior only to [15]. However, [15] used an optimized C++ code to achieve their results. We believe that speed up of computational time is possible with a parallelized optimized code in GPU environment. A quantitative comparison of different prostate segmentation methodologies is difficult in the absence of a public dataset and standardized evaluation metrics. Nevertheless, to have an overall qualitative estimate of the functioning of our method we have compared with some of the 2D segmentation works in the literature in Table 2. In Table 2 we may consider area overlap and area accuracy equivalent to that of DSC values and average distance equivalent to that of average MAD. Analyzing the results we observe that our mean DSC value is comparable to area overlap accuracy values of Betrouni et al. [3] and Ladak et al. [11] and very close to the area overlap error of Shen et al. [14]. However, it is to be noted that we have used more images compared to Shen et al. Our MAD value is comparable to [3], [14],

Table 2. Qualitative comparison of prostate segmentation

Reference	**Area Accuracy**	**Contour Accuracy**	**Datasets**	**Time**
Betrouni [3]	Overlap 93±0.9%	Distance 3.77±1.3 pixels	10 images	5 seconds
Shen [14]	Error 3.98±0.97%	Distance 3.2±0.87 pixels	8 images	64 seconds
Ladak [11]	Accuracy 90.1±3.2%	MAD 4.4±1.8 pixels	117 images	-
Cosio [6]	-	MAD 1.65±0.67 mm	22 images	11 minutes
Yan [15]	-	MAD 2.10±1.02 mm	19 datasets/ 301 images	0.3 seconds
Our Method	DSC 0.97±0.01	MAD 1.82±0.76 pixels/ 0.49±0.20 mm	23 datasets/ 46 images	5.9 seconds

[11], [6] and [15]. From these observations we may conclude that qualitatively our method performs well in overlap and contour accuracy measures.

4 Conclusion and Future Works

A novel approach of multiple statistical models of shape and posterior probability information of prostate region with the goal of segmenting the prostate in 2D TRUS images has been proposed. Our approach is accurate, and robust to significant shape, size and contrast variations in TRUS images compared to traditional AAM. While the proposed method is validated with prostate mid gland images, effectiveness of the method against base and apical slices is yet to be validated.

Acknowledgements

This research has been funded by VALTEC 08-1-0039 of Generalitat de Catalunya, Spain and Conseil Régional de Bourgogne, France.

References

1. Prostate Cancer Statistics - Key Facts. info.cancerresearchuk.org/cancerstats/types/prostate, accessed on [6th June, 2011] (2011)
2. Badiei, S., Salcudean, S.E., Varah, J., Morris, W.J.: Prostate Segmentation in 2D Ultrasound Images Using Image Warping and Ellipse Fitting. In: Larsen, R., Nielsen, M., Sporring, J. (eds.) Medical Image Computing and Computer-Assisted Intervention - MICCAI. pp. 17–24. Springer, Berlin and Heidelberg and New York (2006)
3. Betrouni, N., Vermandel, M., Pasquier, D., Maouche, S., Rousseau, J.: Segmentation of Abdominal Ultrasound Images of the Prostate Using A priori Information and an Adapted Noise Filter. Computerized Medical Imaging and Graphics 29, 43–51 (2005)

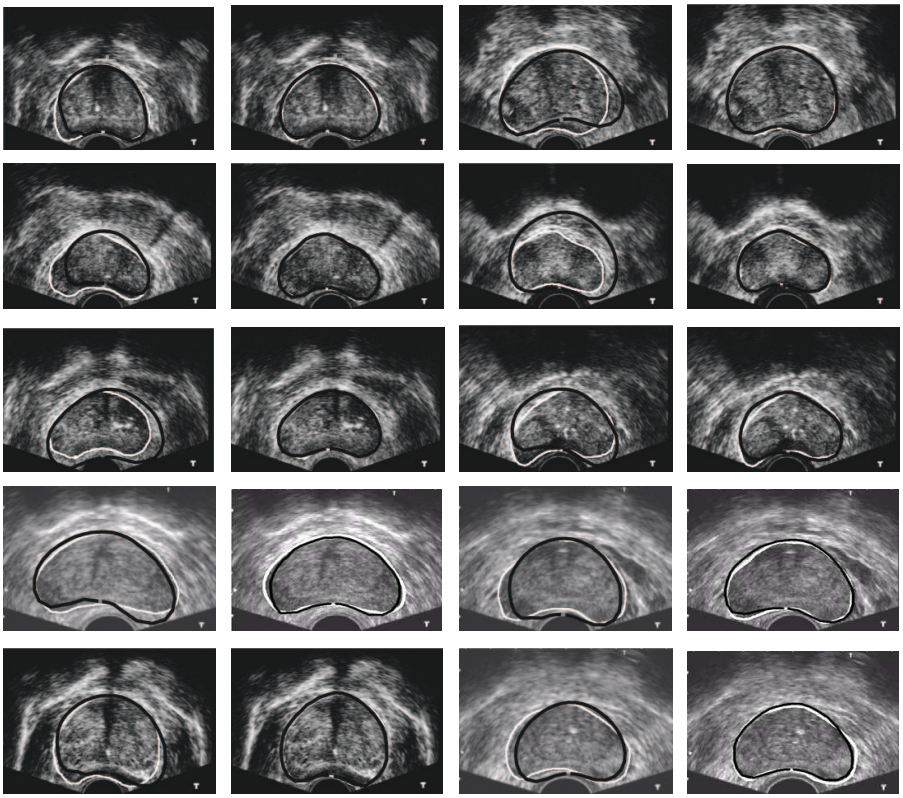

Fig. 4. Performance of our algorithm against shape, size and contrast variations. The white contour gives the ground truth and the black contour gives the obtained result. Columns 1, and 3 show segmentations with traditional AAM and 2, and 4 show corresponding segmentations with our model for 10 datasets.

4. Cootes, T.F., Hill, A., Taylor, C.J., Haslam, J.: The Use of Active Shape Model for Locating Structures in Medical Images. Image and Vision Computing 12, 355–366 (1994)
5. Cootes, T., Edwards, G., Taylor, C.: Active Appearance Models. In: H.Burkhardt, Neumann, B. (eds.) In Proceedings of European Conference on Computer Vision. pp. 484–498. Springer, Berlin and Heidelberg and New York (1998)
6. Cosío, F.A.: Automatic Initialization of an Active Shape Model of the Prostate. Medical Image Analysis 12, 469–483 (2008)
7. Diaz, K., Castaneda, B.: Semi-automated Segmentation of the Prostate Gland Boundary in Ultrasound Images Using a Machine Learning Approach. In: Reinhardt, J.M., Pluim, J.P.W. (eds.) Procedings of SPIE Medical Imaging : Image Processing. pp. 1–8. SPIE, USA (2008)
8. Duda, R.O., Hart, P.E., Stork, D.G.: Pattern Classification. Wiley-Interscience, USA, second edn. (2000)
9. Ghose, S., Oliver, A., Martí, R., Lladó, X., Freixenet, J., Vilanova, J.C., Meriaudeau, F.: Texture Guided Active Appearance Model Propagation for Prostate

Segmentation. Book Series Lecture Notes in Computer Science Springer 6367, 111–120 (2010)
10. Gower, J.C.: Generalized Procrustes Analysis. Psychometrika 40, 33–51 (1975)
11. Ladak, H.M., Mao, F., Wang, Y., Downey, D.B., Steinman, D.A., Fenster, A.: Prostate Segmentation from 2D Ultrasound Images. In: Proceedings of the 22nd Annual International Conference of the IEEE Engineering in Medicine and Biology Society. pp. 3188–3191. IEEE Computer Society Press, Chcago, USA (2000)
12. Liu, H., Cheng, G., Rubens, D., Strang, J.G., Liao, L., Brasacchio, R., Messing, E., Yu', Y.: Automatic Segmentation of Prostate Boundaries in Transrectal Ultrasound (TRUS) Imaging. In: Sonka, M., Fitzpatrick, J.M. (eds.) Proceedings of the SPIE Medical Imaging : Image Processings. pp. 412–423. SPIE, USA (2002)
13. MICCAI: 2009 prostate segmentation challenge MICCAI. http://wiki.namic.org/Wiki/index.php, accessed on [1st April, 2011] (2009)
14. Shen, D., Zhan, Y., Davatzikos, C.: Segmentation of Prostate Boundaries from Ultrasound Images Using Statistical Shape Model. IEEE Transactions on Medical Imaging 22, 539–551 (2003)
15. Yan, P., Xu, S., Turkbey, B., Kruecker, J.: Discrete Deformable Model Guided by Partial Active Shape Model for TRUS Image Segmentation. IEEE Transactions on Biomedical Engineering 57, 1158–1166 (2010)
16. Zhan, Y., Shen, D.: Deformable Segmentation of 3D Ultrasound Prostate Images Using Statistical Texture Matching Method. IEEE Transactions on Medical Imaging 25, 256–272 (2006)